1 Title

2 Single cell analysis reveals modified hematopoietic cell composition affecting inflammatory and
3 immunopathological responses in *Astyanax mexicanus*

4 Authors

5 Robert Peuß[1], Andrew C. Box[1], Yongfu Wang[1], Shiyuan Chen[1], Jaya Krishnan[1], Dai Tsuchiya[1],
6 Brian Slaughter[1] & Nicolas Rohner[1,2]

7 Author for correspondence:

8 Nicolas Rohner (nro@stowers.org)

9

10 Affiliation

11 [1] Stowers Institute for Medical Research, Kansas City, MO, USA

12 [2] Department of Molecular & Integrative Physiology, KU Medical Center, Kansas City, KS, USA
13

14

15 Abstract

16 Reduction of parasite diversity in modern human populations is suspected to be a primary cause
17 for the increase of autoimmune disorders. However, the long-term evolutionary consequences of
18 decreased parasite diversity on the host immune system are not well understood. We used the
19 cavefish *Astyanax mexicanus* to understand how loss of biodiversity, a hallmark of cave
20 adaptation, influences the evolutionary trajectory of the vertebrate host immune system by
21 comparing river with cave morphotypes. We show that cavefish display a more sensitive
22 proinflammatory immune response towards bacterial endotoxins, which is characteristic in other

vertebrate species inhabiting environments with decreased biodiversity. Surprisingly, cellular immune responses, such as phagocytosis, are drastically decreased in cavefish. Using an image-based immune cell phenotyping approach and single-cell RNA sequencing, we identified a shift in the overall immune cell composition in cavefish as the underlying cellular mechanism associated with altered immune responses. The shift results in an overall decrease of immune cells mediating inflammation *in -vivo* and cellular immune responses such as phagocytosis (i.e. neutrophils and monocytes). Moreover, we find that immunopathological phenotypes in visceral adipose tissue are drastically reduced in cavefish. Our data indicate that a more sensitive immune system in cavefish is compensated by a reduction of the immune cells that play a role in mediating the proinflammatory response. These findings reveal that cavefish are an effective model system to study the evolution of auto-inflammatory processes.

35 Main text

36 Important efforts in hygiene and medical treatment in most industrialized countries have reduced
37 microbial and parasitic infections considerably [1]. While this indisputably improves health and
38 increases life expectancy, the diverse effects on the host immune system are not understood. It
39 has been hypothesized that decreased exposure to parasites or biodiversity in general has
40 contributed to the rising numbers of autoimmune diseases in the developed world [2-5]. This
41 phenomenon has been described as the “Old Friends hypothesis” [6], which argues that the
42 vertebrate host immune system depends upon the exposure to certain parasites (macroparasites
43 (i.e., helminths) and microparasites (i.e., bacteria and fungi)). These parasites, that the host has
44 coevolved with, are necessary for the host to develop a proper functional immune system and to
45 avoid autoimmune reactions that potentially result in immunopathology (e.g. type 1 diabetes or
46 artheriosclerosis) [6]. Despite important insights into the physiological underpinnings of
47 autoimmune diseases [7], we still lack fundamental knowledge of how autoimmune diseases
48 initially develop. Given the significant impact on fitness of autoimmune disorders [7], evolutionary
49 adaptation to environments with low biodiversity and thereby low parasite diversity [8, 9] are likely
50 to have been deployed to compensate these negative effects. To explore this idea, we utilized an
51 eco-immunological approach in the Mexican tetra *Astyanax mexicanus*, to study how local
52 adaptation of one host species to environments with a stark difference in parasite diversity affects
53 the immune system of the host. There are cave and surface adapted populations of this species
54 that have adapted to their respective environments for approximately 200 thousand years [10].
55 One important hallmark of cave environments is an overall decrease in biodiversity, including
56 parasite diversity [11, 12]. These fish can be bred and raised for generations in the lab under
57 identical environmental conditions, which readily facilitates the identification of heritable changes.
58 We demonstrate that cavefish show a more sensitive and prolonged immune response of
59 proinflammatory cytokines towards bacterial endotoxins *in -vitro* and *in -vivo,* similar to other

60 vertebrate host species in environments with low biodiversity [13, 14]. However, using an image-
61 based immune cell clustering approach and single cell RNA sequencing we show that the
62 observed sensitivity towards bacterial endotoxins is accompanied by a reduction of immune cells
63 in the myeloid cell linage, such as monocytes and neutrophils, which are indispensable for
64 proinflammatory processes [15]. This reduction of the myeloid cell linage in the main
65 hematopoietic organ is presumably caused by a shift in hematopoiesis towards the lymphoid
66 lineages and / or myeloid erythroid progenitors. We demonstrate that with the reduction of
67 monocytes and neutrophils, the *in -vivo* proinflammatory responses and the immunopathological
68 consequences (i.e. sites of inflammation) for elevated fat storage are drastically reduced in
69 cavefish.

70 To explore differences in the potential to develop immunopathological phenotypes between
71 surface fish and cavefish (Pachón cave), we first investigated whether we can detect differences
72 in the proinflammatory immune response, which generally precedes immunopathological
73 phenotypes [16]. To trigger such a proinflammatory immune response we used bacterial
74 endotoxins (lipopolysaccharides, LPS). We focused on the main hematopoietic organ, the
75 pronephros (head kidney, HK) (Figure 1a), a major lymphoid organ and a site of antigen
76 representation in teleost fish [17]. We incubated head kidney cells with LPS (20 µg/mL) for 1, 3,
77 6, 12 and 24 hours, respectively and measured gene expression of the proinflammatory cytokines
78 *il-1β*, *tnf-α*, *il-6 and g-csf* using RT-qPCR (Figure 1b,c, see Table S1 for details). Hematopoietic
79 cells from cavefish show an overall greater inducible response upon LPS treatment than
80 hematopoietic cells from surface fish *in -vitro* (Fig. 1b). Specifically, only the gene expression in
81 *il-1β* remains significant in surface fish after 24 hours (Figure 1b). In contrast, in cavefish
82 expression of all tested proinflammatory cytokine remains highly significantly upregulated after 24
83 hrs. Since the cavefish response was saturated at this LPS concentration, we repeated the
84 analysis with a 100x fold lower LPS exposure (Fig. 1c). Again, LPS treated cavefish cells showed

significant expression for *il-1β*, *tnf-α and il-6* compared to untreated cells, while hematopoietic cells of surface fish no longer displayed a significant response of any of the proinflammatory cytokines (Figure 1c). To test the inducible inflammatory response *in -vivo*, we injected adult surface fish and cavefish with 20 µg LPS per g bodyweight and compared them to fish injected with PBS.

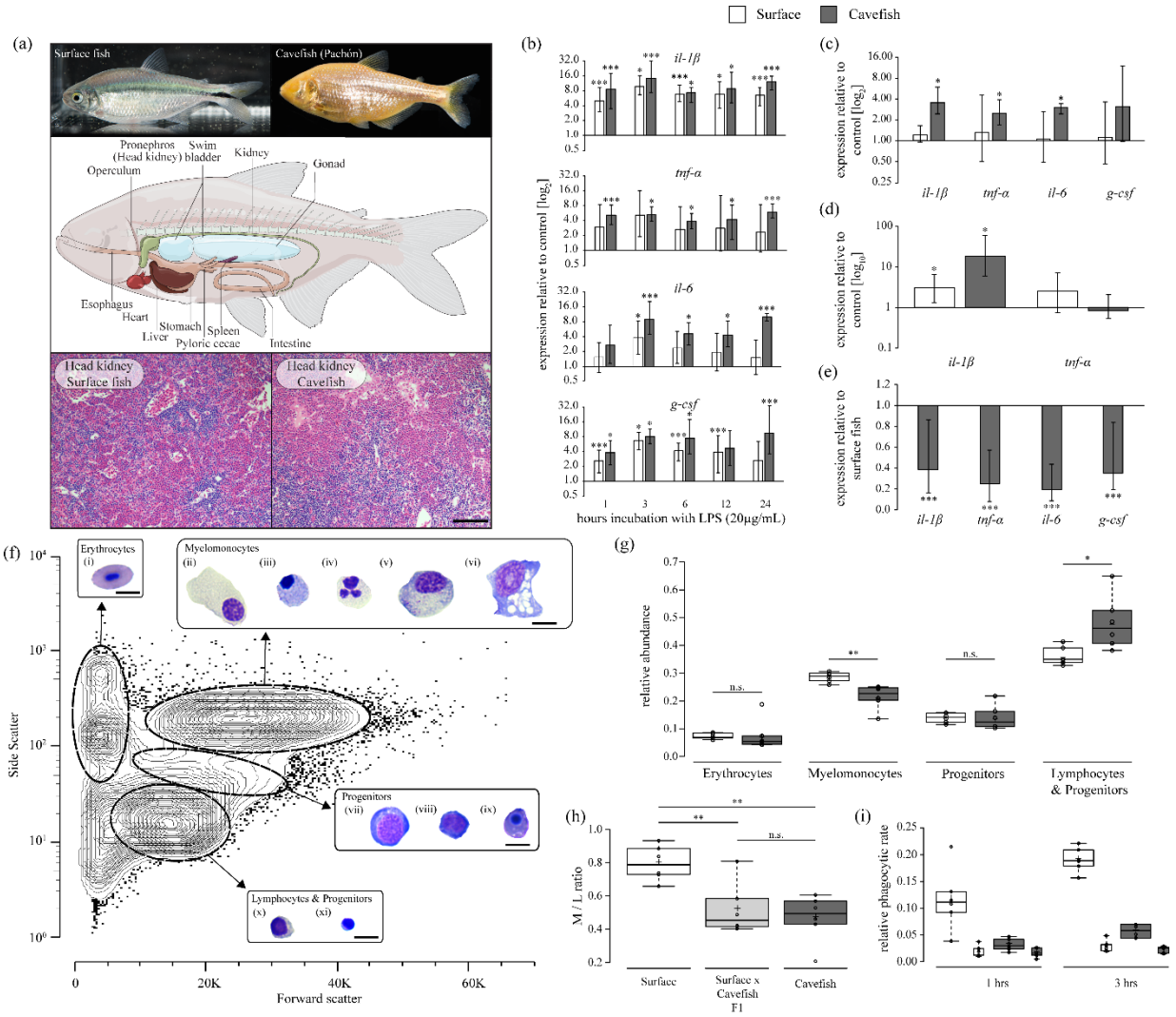

*Fig. 1 Cavefish show an increased sensitivity of proinflammatory responses and decreased baseline immune function caused by changes of the hematopoietic cell composition. (**a**) Adult surface and cave morphotype (Pachón) of A. mexicanus; cartoon indicates anatomical position of the main hematopoietic organ, the head kidney and below are H & E stained section of the head kidney from each morphotype (scale bar is 100 µm). (**b-c**) RT-qPCR analysis of pro-inflammatory cytokines, interleukin-1beta (il-1β), tumor necrosis factor alpha (tnf-α), interleukin-6 (il-6) and granulocyte colony stimulating factor (g-csf), of HK cells from surface and cavefish after incubation with (b) 20 µg/mL lipopolysaccharide (LPS) or (c) 0.2 µg/mL LPS relative to HK cells incubated without LPS. Plotted is the mean of three independent experiments with standard error (SE) (**d**) RT-qPCR analysis of proinflammatory cytokines il-1β & tnf-α after intraperitoneal injection of LPS in vivo (20 µg/ g (bodyweight fish)). N=5 and 4 for surface fish and cavefish, respectively. (**e**) RT-qPCR based expression analysis of proinflammatory cytokines il-1β, tnf-α, il-6, g-csf of cavefish relative to surface fish of control samples across all timepoints as shown in (b) and (c) (n=18). Significance values were determined by a pairwise fixed reallocation randomization test using REST2009 software [18]. (**f**) Representative*

*contour plot of HK cells from three surface A. mexicanus after FACS analysis using scatter characteristics showing 99 % of all events. 4 different population (erythrocytes, myelomonocytes, progenitors and lymphocytes & progenitors) were identified and sorted for May-Grünwald Giemsa staining. Images of representative cells that were found in each population are shown for each population and identified based on similar approaches in zebrafish [17, 19] as (i) mature erythrocytes, (ii) promyelocytes, (iii) eosinophiles, (iv) neutrophiles, (v) monocytes, (vi) macrophages, (vii) erythroblasts, (viii) myeloblasts, (ix) erythroid progenitors, (x) lymphocytes and (xi) undifferentiated progenitors. Scale bar is 10 µm. (**g**) Box plots of relative abundances of HK cells from surface and cavefish within the 4 population as defined by scatter characteristics in (f) for six independent replicates for surface and cavefish respectively. Significances were determined by one-way ANOVA and subsequent FDR. (**h**) Box plot representation of myelomonocyte / lymphocyte (M / L) ratio from surface, surface x cavefish F1 hybrids and cavefish (n=6 for each). (**i**) Box plot presentation of relative phagocytic rate of HK cells from surface fish and cavefish incubated with Alexa-488 coupled Staphylococcus aureus. To control for passive uptake of Alexa-488 coupled S. aureus, a control sample was incubated with Alexa-488 coupled S. aureus in the presence of 80 µg cytochalasin B (CCB) and phagocytic rate is presented in small boxes of the same color of the respective fish population and timepoint. Significant differences between surface and cavefish for each timepoint across six independent experiments were determined by two-way Anova (see Table S2 for statistical details). For all box plots; center lines show the medians, crosses show means; box limits indicate the 25th and 75th percentiles as determined by R software [20]; whiskers extend 1.5 times the interquartile range from the 25th and 75th percentiles, data points are represented by circles. Significances are indicated as * for p ≤ 0.05; ** for p ≤ 0.01 and *** for p ≤ 0.001 for all experiments.*

We monitored the relative inflammatory response by analysing gene expression of *il-1β* and *tnf-α* in liver tissue 24 hours post injection using RT-qPCR (Figure 1d). While we did not detect a significant difference in *tnf-α* expression, the main proinflammatory cytokine *il-1β* was highly increased in LPS treated cavefish compared to PBS injected controls (expression of *il-1β* = 18.976 relative to PBS injected fish, $p \leq 0.05$, *pairwise fixed reallocation randomization test,* Fig. 1d). In contrast, surface fish showed a weaker response (expression of *il-1β* = 3.185 relative to PBS injected fish, $p \leq 0.05$, *pairwise fixed reallocation randomization test,* Fig. 1d). This increased sensitivity of cavefish hematopoietic cells towards LPS *in -vivo* and *in -vitro* is supported by previous findings of an increased immune and scarring response after wounding of the Pachón cave population compared to surface fish [21]. However, the observed differences in the proinflammatory response could be impacted by the number of cells that produce these proinflammatory cytokines. For example, it is possible that individual immune cells respond similarly to LPS treatment when comparing surface fish and cavefish but the overall cell numbers are changed between these two morphotypes. Therefore we directly compared baseline expression of *il-1β*, *tnf-α*, *il-6 and g-csf* in naïve hematopoietic cells of cavefish and surface fish (Fig. 1e). Surprisingly, the expression of all tested proinflammatory cytokines was significantly reduced in cavefish cells relative to surface fish cells (Fig. 1e). In the case of the proinflammatory

138 cytokine *il-1β*, for example, naïve cavefish hematopoietic cells produced 61 % less transcript than
139 surface fish cells (relative expression cavefish vs. surface fish *il-1β* = 0.383, $p \leq 0.001$, *pairwise*
140 *fixed reallocation randomization test*, Fig. 1e). Since proinflammatory cytokines, such as *il-1β* or
141 *il-6* are mainly produced by cells with myelomonocytic (monocytic or granulocytic cells) origin in
142 teleost fish [19, 22], we tested whether the differences in baseline expression of proinflammatory
143 cytokines between surface and cavefish are due to differences in absolute cell numbers of specific
144 immune cells. To access such differences, we analyzed scatter information from head kidney
145 derived single cell suspensions. We identified four distinct cell populations: an erythroid, a
146 myelomonocyte, a progenitor and a lymphoid/progenitor cluster using similar analytical
147 approaches previously described for zebrafish [19] (Fig. 1f). To confirm the identity of these
148 clusters, hematopoietic cells from each cluster were sorted, and cells were stained with May-
149 Grünwald Giemsa stain. Based on comparative morphological analysis in zebrafish [23], we
150 identified (i) erythrocytes, (ii) promyelocytes, (iii) eosinophiles, (iv) neutrophiles, (v) monocytes,
151 (vi) macrophages, (vii) erythroblasts, (viii) myeloblasts, (ix) erythroid progenitors, (x) lymphocytes
152 and (xi) undifferentiated progenitors (i.e. hematopoietic stem cells, common lymphoid progenitors
153 and common myeloid progenitors) within the four cell clusters (Fig. 1f). We observed no general
154 differences in cell morphology between surface fish and cavefish. While we did not detect
155 significant changes in the absolute numbers of hematopoietic cells from the entire head kidney
156 between the fish populations (mean absolute cell number of entire head kidney per mg fish weight
157 for surface fish (n=12) was 8556 and 7460 for cavefish (n=12), $p = 0.53$ one-way ANOVA, see
158 Fig. S1), surface fish and cavefish cell numbers differed significantly in 2 of the 4 clusters (Fig.
159 1g). There are fewer myelomonocytic cells in cavefish (mean relative abundance of cells in
160 myelomonocyte cluster in surface fish is 0.286 vs. 0.214 in cavefish, $p \leq 0.01$, one-way ANOVA,
161 FDR corrected, Fig. 1g) and an increased number of cells in the lymphocyte & progenitor cluster
162 (mean relative abundance of cells in lymphocyte & progenitor cluster in surface fish is 0.362 vs.
163 0.481 in cavefish, $p \leq 0.05$, one-way ANOVA, FDR corrected, Fig. 1g). When we used these

164 relative abundances to calculate the myelomonocyte / lymphocyte (M / L) ratio, which is an
165 indication of an individuals relative investment in either innate (myelomonocyte) or adaptive
166 (lymphocyte) immune cell populations [24], we found strong differences in the immune investment
167 strategy between surface and cavefish (Fig. 1h). While surface fish have a relatively balanced
168 investment in myelomonocyte and lymphoid immune cells, cavefish invest less into
169 myelomonocytic cells than into lymphoid immune cell populations (mean M / L ratio in surface fish
170 is 0.80 vs. 0.47 in cavefish, $p \leq 0.01$, one-way ANOVA, FDR corrected, Fig. 1h). Since all fish
171 were raised under identical conditions this indicates a genetic basis. To get some insight into the
172 genetic architecture of the trait, we analysed surface x cavefish hybrids and found a similar M / L
173 ratio as in the cavefish population indicating that the decreased investment into myelomonocytes
174 of the cavefish may be a dominant trait (mean M / L ratio in surface x cavefish F1 is 0.52, $p \leq 0.01$
175 and $p = 0.56$ when compared to surface and cavefish population, respectively, one-way ANOVA,
176 FDR corrected, Fig. 1h). We hypothesized that other cellular immune functions, such as
177 phagocytosis, which are mainly performed by myelomonocytes [25] should be reduced as well.
178 To test this, we conducted a phagocytosis experiment in which we quantified the ability of
179 hematopoietic cells to phagocytize Alexa-488 tagged *Staphylococcus aureus* cells (Thermo
180 Fisher) *in -vitro*. We found significantly lower rates of phagocytosing cells in cavefish compared
181 to surface fish (Fig. 1i, significance of population $p \leq 0.0001$, $F(1, 10) = 59.98$, two-way ANOVA,
182 see Table S2 for details). After 1 hr incubation with bacteria, the mean phagocytic rate was 0.032
183 in cavefish and 0.117 in surface fish and after 3 hrs incubation the median phagocytic rate was
184 0.054 in cavefish and 0.186 for surface fish (Fig. 1i, Table S2). Given this difference in cytokine
185 expression, M/L ratio and the ability to phagocytose bacteria, we chose to analyze the immune
186 cell composition on a single cell basis of both surface fish and cave-dwelling fish to investigate

187 whether these changes are due to changes in immune cell composition of the hematopoietic
188 organ.

189 We clustered hematopoietic cells based on cell morphology by using image-based cytometry and
190 advanced clustering algorithms [26]. The method is a semi-unsupervised, high content image-
191 based cell analysis independent of cell specific antibodies or the assumption that specific immune
192 cells express certain genes. This makes it an effective method for organisms lacking established
193 transgenic lines or antibodies to identify specific immune cell populations. This approach allows
194 immune cells to be clustered based on their morphology, independent of observer bias that has
195 been reported for such analysis [27]. First, we sorted myelomonocyte, lymphocyte and progenitor
196 cell populations as identified in Fig. 1g in order to reduce mature erythrocytes composition in
197 hematopoietic single cell suspensions (see Supplemental Text for details). In total we recorded
198 10,000 nucleated events (i.e., cells) by image cytometry from each replicate surface fish (n=5) or
199 cavefish (n=6) (see supplemental methods for more details) and identified 17 distinct cell clusters
200 (Fig. 2a). The identity of each cluster is based on cell image galleries from each cluster (see Data
201 File 1) in comparison to the histological staining of sorted cells as presented in Fig. 1g. In addition,
202 to verify certain cellular features (e.g., complexity of nuclei, cell shape) within certain cluster, we

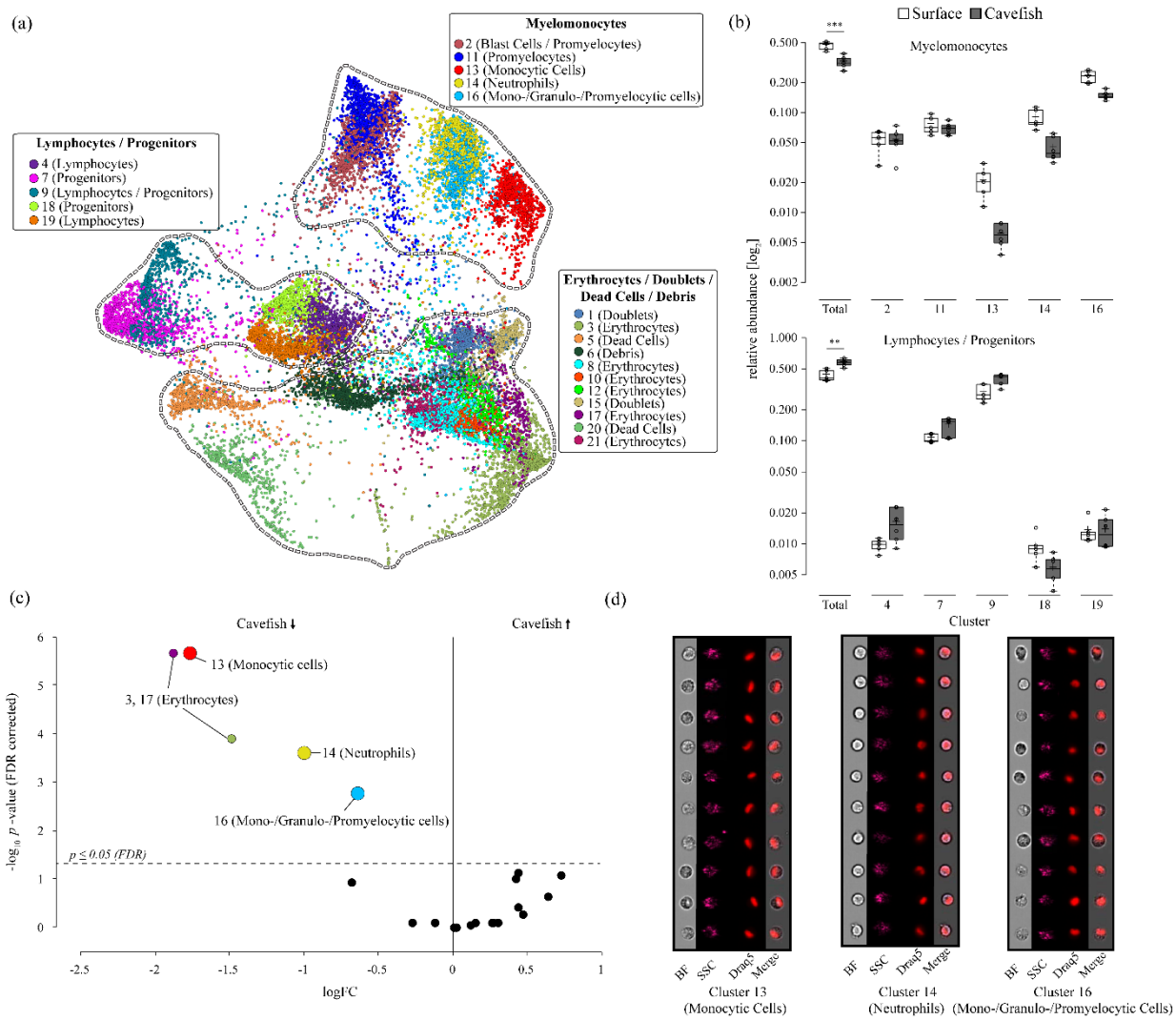

*Fig. 2 Cell composition analysis of A. mexicanus head kidney based on cell morphological features by semi-supervised clustering [26]. (**a**) Force directed layout graph of clusters generated from morphological feature intensities from HK cells of surface fish (n=5) and cavefish (n=6) (see supplemental methods for details). Each color represents a unique cluster. Clusters were combined into 3 super-cluster (Myelomonocytes, Lymphocytes / Progenitors, mature Erythrocytes / Doublets / Debris) based on their morphology (see supplemental methods for details). (**b**) Relative abundances of cells within each cluster of the myelomonocyte and lymphocyte / progenitor super-cluster in relation to all cell included in the analysis of the respective fish. Significant differences in the relative abundance of cells within each category (total) where determined by a one-way ANOVA and subsequent FDR. Significance values are indicated as ** for p ≤ 0.01. For box plots; center lines show the medians, crosses show means; box limits indicate the 25th and 75th percentiles as determined by R software; whiskers extend 1.5 times the interquartile range from the 25th and 75th percentiles, data points are represented by circles. (**c**) Volcano plot of absolute count comparison analysis of all clusters between surface fish and cavefish. Significant differences were determined by negative binominal regression model with subsequent FDR analysis. Cluster that differ significantly between surface fish and cavefish are highlighted in their respective color as shown in (a). (**d**) Representative cell gallery of significant cluster from the myelomonocyte super-cluster as determined in (c). Cluster galleries were produced as described before [26]. Cell galleries show images of brightfield (BF), side scatter (SSC), nuclei (visualized trough nuclei dye Draq5) and merged image of BF and Draq5 (Merge).*

203 used an intensity feature/cluster correlation analysis (Fig. S2). Clusters were assigned to one of

204 the following super-clusters based on their identity: myelomonocytes (cluster 2, 11, 13, 14, 16);

205 lymphocytes/progenitors (cluster 4, 7, 9, 18, 19) and mature erythrocytes/doublets/debris (cluster
206 1, 3, 5, 6, 8, 10, 12, 15, 17, 20, 21) (Fig 2a). In line with the scatter analysis, we found a significant
207 reduction of cells within the myelomonocyte super-cluster in cavefish compared to surface fish
208 (mean relative abundance of 0.468 cells in surface fish vs 0.320 cells in cavefish; $p \leq 0.001$,one-
209 way Anova and FDR correction, Fig. 2b). To identify differences in the absolute cell numbers
210 between surface fish and cavefish in specific clusters we used a negative binomial regression
211 model (Fig. 2c, see Methods for statistical details). Here, monocytic cells (cluster 13; logFC = -
212 1.773; $p \leq 0.001$ (FDR corrected)), neutrophils (cluster 14; logFC = –1.003; $p \leq 0.001$ (FDR
213 corrected)) and monocytic-, granulocytic- and promyelocytic cells (cluster 16 logFC = -0.640; $p \leq$
214 0.01 (FDR corrected)) are all significantly underrepresented in cavefish (Fig. 2c). The identity of
215 these three clusters is shown in Fig. 2d. The significant difference in clusters 13 and 16 (mature
216 erythrocytes) initially observed were not significant after combining all erythrocyte clusters
217 (relative abundance of erythrocytes across all clusters was 0.045 in surface fish vs. 0.033 in
218 cavefish, $p = 0.244$, one way ANOVA, FDR corrected). The high number of clusters containing
219 erythrocytes is due to their biconcave shape, which produces different images depending on their
220 orientation as described before [26] (see also supplemental text for details).

221 Such reduction of granulocytes and monocytes in cavefish could account for the decreased
222 baseline expression of proinflammatory cytokines and the reduced phagocytic rate of cavefish
223 head kidney cells. Further, we found that cells within the lymphocyte/progenitor category (Fig. 2a)
224 are generally overrepresented in cavefish when compared to surface fish (mean relative
225 abundance of cells within lymphocytes/progenitors category: surface fish 0.433 vs. cavefish
226 0.580; $p \leq 0.01$ one-way Anova, FDR corrected, Fig. 2b). The major branches in hematopoiesis
227 are the granulocyte-monocyte progenitor (GMP) lineage, the common lymphoid progenitor (CLP)
228 lineage and the erythroid-myeloid progenitor (EMP) lineage. These results suggest a
229 developmental switch in hematopoiesis in cavefish from GMP to CLP and/or EMP. However,

230 using the morphological data alone, we were unable to distinguish between early progenitor cells
231 of hematopoietic lineages and/or lymphocytes (B- and T- cells) due to their high similarities in cell
232 morphology (see Data File 1).

233 We took a genetic approach to resolve whether the difference in the GMP lineage is due to a shift
234 in hematopoiesis in cavefish towards other hematopoietic lineages. We performed single-cell
235 RNA sequencing of all non-mature erythrocytes, FACS-sorted from the head kidney. We used
236 one female adult surface fish and an age, size and sex- matched Pachón cavefish and we
237 identified all major cell types of the hematopoietic organ (Fig. 3a). Based on gene expression
238 analysis, we identified 16 distinct cluster (see Data File 2, Fig. S4), which we grouped into 4
239 categories: myelomonocytes, B-lymphocytes, T-lymphocytes and progenitor cells (Fig. 3a, see
240 Methods for detail). Consistent with the morphological analyses, we found a significant reduction
241 of myelomonocytes in cavefish compared to surface fish (relative abundance of *pu.1*$^{+}$ cells in
242 surface fish 0.231 vs. 0.133 in cavefish, Fig. 3b). Furthermore, we verified the reduction of
243 neutrophils (relative abundance of *cd45*$^{+}$ + *mpx*$^{+}$ + *csf3r*$^{+}$ cells in surface fish 0.078 vs. 0.035 in
244 cavefish, Figure 3b) and monocytes (relative abundance of *cd45*$^{+}$ + *cd74a*$^{+}$ + *csf3r*$^{+}$ cells in
245 surface fish 0.012 vs. 0.006 in cavefish, Fig. 3b). To determine whether this result is due to a shift
246 in hematopoiesis towards other hematopoietic lineages we analysed the relative abundance of
247 hematopoietic stem cells (HSCs) and lymphoid cells. While we detected no change in the relative
248 abundance of HSCs (combined relative abundance of *myb*$^{+}$; *gata2b*$^{+}$; *ctnnb1*$^{+}$ cells in surface fish
249 0.119 vs. 0.133 in cavefish, Fig. S3), we found a strong increase of erythroid myeloid precursor
250 in cavefish (relative abundance of *klf1*$^{+}$ + *epoR*$^{+}$ cells in surface fish 0.003 vs. 0.047 in cavefish,
251 Fig. 3b). This may represent an adaptational response towards low oxygen in the cave

environment [28]. Additionally, we found a strong increase in the relative abundance of lymphocytes in cavefish compared to surface fish (relative abundance of B-and T-cells combined

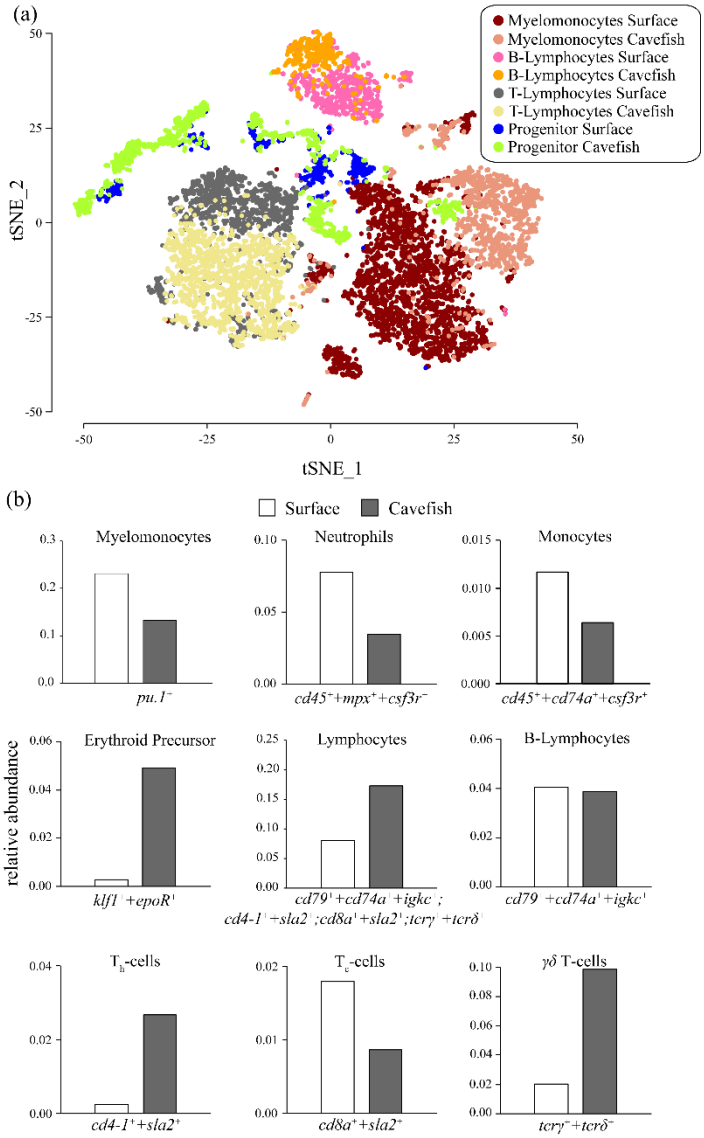

*Fig. 3 Cell composition analysis of A. mexicanus headkidney by single cell RNA sequencing analysis. (**a**) Combined t-SNE plot of surface and cave hematopoietic cells, where each color represents unique category as shown in the legend. For details on clustering and categorization see Supplemental Method section. (**b**) Relative abundance of specific cell population of surface fish and cavefish (Pachón) based on the expression of given gene(s). Cells were assigned to specific population when expressing the respective gene in logFC ≥ 1 in comparison to the overall expression, except for Erythroid Precoursor where logFC ≥ 0 was used.*

in surface fish 0.081 vs. 0.173 in cavefish, Fig. 3b). While we found almost identical relative abundances of B-lymphocytes (relative abundance of *cd79a*⁺ + *cd74a*⁺ + *igkc*⁺ cells in surface fish 0.040 vs. 0.039 in cavefish), we found clear differences in the numbers of HK resident T-cells. While the majority of T-cells in surface fish are T_c-cells (relative abundances of *cd8a*⁺ + *sla2*⁺ in

258 surface fish 0.018, Fig. 3b), T_h-cells are almost absent (relative abundances of *cd4-1*$^+$ + *sla2*$^+$ in
259 surface fish 0.002, Fig. 3b). In contrast, cavefish had lower numbers of T_c-cells (relative
260 abundances of *cd8a*$^+$ + *sla2*$^+$ in cavefish 0.009, Fig. 3b) and higher numbers of T_h-cells (relative
261 abundances of *cd4-1*$^+$ + *sla2*$^+$ in cavefish 0.020, Fig. 3b). We also identified increased numbers
262 of $\gamma^+\delta^+$CD4$^-$ CD8$^-$ (*γδ*) T-cells residing in the headkidney of cavefish (relative abundances of *tcrγ*$^+$
263 + *tcrδ*$^+$ in cavefish 0.099, Fig. 3b), while the relative abundance of *γδ* - T-cells in surface fish was
264 relatively low and comparable to the numbers of T_c-cells (relative abundances of *tcrγ*$^+$ + *tcrδ*$^+$ in
265 surface fish 0.020, Fig. 3b). Although this innate T-cell population has only been discovered
266 recently in other teleost species [29], it is interesting to note, that *γδ* T-cells$^-$ were reported to play
267 a significant role in homeostasis and inflammation of mammalian adipose tissue [30]. In mice for
268 example, *γδ* T-cell number increase proportionally with the mass of adipose tissue [31]. *γδ* T-cells
269 may play a similar role in *A. mexicanus* and given the increased fat storage in cavefish [32], *A.*
270 *mexicanus* seems like a good model to study the function of *γδ* T-cells. Taken together, we
271 confirmed a reduction of hematopietic cells in the GMP lineage of cavefish, likely due to a shift
272 towards the EMP and / or CLP lineage. The reduction of monocytes and neutrophils in the main
273 hematopoietic organ raises the question as to whether this has direct consequences for the
274 inflammatory response of the cavefish *in -vivo*.

275 Hematopoietic cells from cavefish are more sensitive towards LPS based on the expression of
276 proinflammatory cytokines, such as IL-1β, *in -vitro* and *in -vivo* (see Fig. 1b, c and d). The
277 reduction of cells in the GMP lineage in hematopoietic tissue could therefore act as a
278 compensatory mechanism to reduce immunopathological consequences of a more sensitive
279 immune system. To test this hypothesis, we injected surface fish and cavefish with 20 µg/ g
280 (bodyweight) LPS and after 3 hours dissected the head kidney and spleen to visualize the
281 expression of *il-1β in -situ* using RNAscope (see Methods section for details). LPS injected
282 surface fish showed a relatively high number of *il-1β* positive cells in the HK compared to cavefish

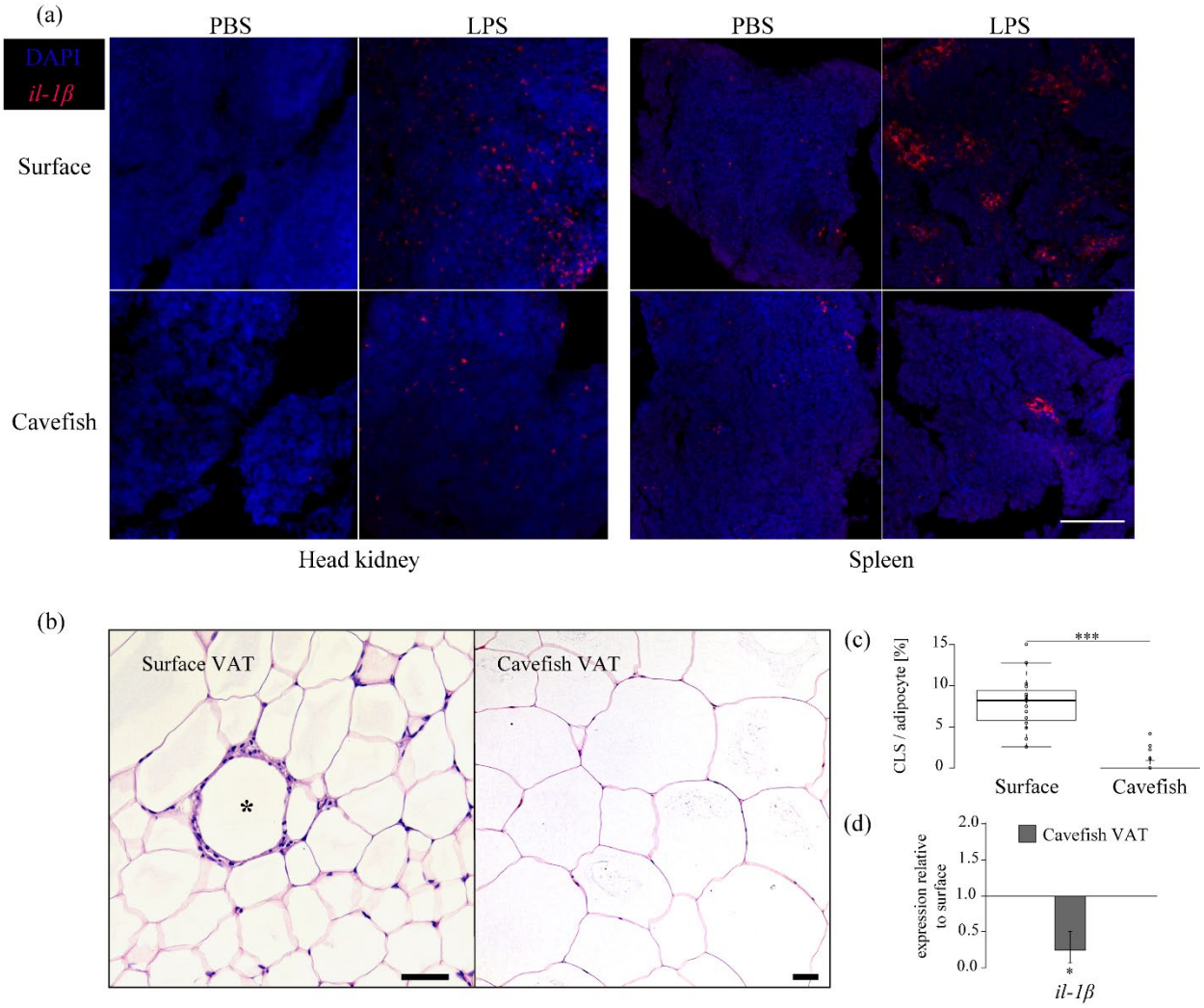

*Fig. 4 Monocyte and neutrophil reduction alter inflammatory and immunopathological response of A. mexicanus. (**a**) In-vivo inflammatory response displayed by in-situ staining of il-1β using RNAscope in head kidney and spleen of surface fish and cavefish (Pachón) 3 hours post intraperinoteal injection of LPS 20 µg/g(bodyweight). Images are representative of two independent experiments. Scale bar is 300 µm (**b**) H & E staining of visceral adipose tissue (VAT) of surface fish and cavefish. Crown-like structure (CLS) is indicated as * in surface VAT. Scale bar is 50 µm. (**c**) CLS count per 100 adipocytes in VAT of surface fish and cavefish in at least three fields of view for each fish (n=3). Significance values were determined by one-way ANOVA. For all box plots; center lines show the medians, crosses show means; box limits indicate the 25th and 75th percentiles as determined by R software* [20]*; whiskers extend 1.5 times the interquartile range from the 25th and 75th percentiles, data points are represented by circles. Significance values are indicated *** for p ≤ 0.001. (**d**) Gene expression of il-1β in cavefish VAT relative to surface fish of the same fish that were used for (c). Significance values were determined by a pairwise fixed reallocation randomization test using REST2009 software* [18] *and are indicated as * for p ≤ 0.05.*

283 (Fig. 4a). In teleost fish, the spleen contains high numbers of mononuclear phagocytes, i.e.
284 macrophages [19] but is generally not a hematopoietic tissue for such cell types [33]. Similar to
285 the head kidney, we observed considerably fewer cells that express *il-1β* after injection with LPS
286 in the spleen from cavefish compared to surface fish (Fig. 4a). We used RNAscope on dissociated

287 head kidney cells from surface fish 3hpi with LPS to validate that mainly cells with monocytic
288 characteristics (large kidney shape nuclei) express *il-1β* (Fig. S5).

289 Based on these results, we hypothesized that the lack of a systemic proinflammatory response in
290 cavefish upon exposure to an immune stimulant (i.e., LPS) *in -vivo* leads to a decreased presence
291 of immunopathological phenotypes that result from such inflammatory responses. Cavefish
292 produce substantially more visceral adipose tissue (VAT) than surface fish [32]. In mammals, the
293 amount of VAT is positively correlated with number of monocytes infiltrating the adipose tissue
294 and mediating inflammatory processes resulting in the formation of crown-like structures (CLS)
295 [34]. Therefore, we tested whether VAT of *A. mexicanus* shows signs of CLS and if surface fish
296 and cavefish differ in their occurrence. We detected CLS in the visceral adipose tissue of surface
297 fish (Fig. 4b), but not in cavefish, despite the prevalence of large, hypertrophic adipocytes
298 (average numbers of CLS in 100 adipocytes were 7.95 for surface vs. 0.6 for cavefish, $p \leq 0.001$,
299 one-way ANOVA, Fig. 4c). To measure levels of *il-1β* expression, we took a sub-sample of the
300 VAT for RT-qPCR analysis. As for the hematopietic cells (Fig. 1e), *il-1β* expression is significantly
301 reduced in VAT of cavefish relatively to surface fish (mean relative expression of cavefish
302 compared with surface fish 0.249, $p \leq 0.05$, pairwise fixed reallocation randomization test, Fig.
303 4d). In combination with the reduced number of CLS, our data indicate a reduction of monocytic
304 cells in VAT of cavefish enabling increased VAT storage in cavefish without immunopathological
305 consequences.

306 Our study elucidates how cave adaptation affects the immune system of a vertebrate host. The
307 Pachón cavefish population of *A. mexicanus* shows a more sensitive proinflammatory immune
308 response similar to other vertebrate hosts in environments with low biodiversity [13]. The loss of
309 monocytes and neutrophils, is potentially due to a shift in hematopoiesis from GMP to the EMP
310 and / or CLP lineage, and given that the immune system is costly in terms of fitness [35], it is likely
311 to be a consequence of the loss of parasite diversity in the cave environment. Here it is noteworthy

312 that relative numbers of granulocytes in wild stickleback populations, for example, positively
313 correlate with diversity of macroparasites these fish were infected with [36]. Proinflammatory
314 reactions are one of the main causes for immunopathological phenotypes and have a tremendous
315 impact on the fitness of an organism and can be caused by a variety of environmental factors [37-
316 39]. From an evolutionary perspective, we therefore interpreted the reduction of cells in the GMP
317 lineage, which mediate these proinflammatory processes but also act against parasites, as an
318 adaptational response of cavefish to decrease the immunopathological consequences from an
319 increased immune sensitivity in an environment with low parasite diversity. The reduced numbers
320 of cells in cavefish that mount a proinflammatory response might come with a potential fitness
321 cost when confronted with a pathogen, which needs to be elaborated in further studies. One
322 fitness advantage we demonstrate here is that the reduction of monocytes and neutrophils seems
323 to enable the cavefish to store increased amounts of VAT, which we interpret as an adaption
324 towards seasonality of food supply. These results position *A. mexicanus* as a unique and novel
325 model to study the impact of parasite diversity on the evolutionary trajectory of the host immune
326 system and identify the genetic basis for immunological sensitivity and immunopathology.

327

328 <u>Acknowledgements</u>

329 We are grateful to the cavefish facility staff at the Stowers Institute for support and husbandry of
330 the fish. We would like to thank the staff from the Histology core at the Stowers Institute for their
331 technical support, Jillian Blanck from the Cytometry core for performing the sorting of
332 hematopoietic cells, Michael Peterson, Allison Peak and Anoja Perera for the scRNA-seq support,
333 Mark Miller for his support on the fish anatomy figure and Hua Li for her support on the statistical
334 analysis. The authors also kindly acknowledge Joachim Kurtz and Jörn Scharsack for helpful
335 discussions. NR was supported by institutional funding, the Edward Mallinckrodt foundation and

the JDRF. RP was supported by a grant from the Deutsche Forschungsgemeinschaft (PE 2807/1-1).

Author Contributions

RP and NR conceived of the study. RP designed and coordinated the experiments with support from ACB and JK. RP performed and analysed immune assays, flow cytometry experiments and histological analysis with support from ACB, YW and DT. SC performed single cell sequencing analysis with support from RP. RNAscope experiments and analysis were performed by YW, DT and BS with support from RP and JK. RP and NR designed and RP made the figures. RP and NR wrote the paper and all authors read and edited the paper.

Data availability statement

Original data underlying this manuscript can be accessed from the Stowers Original Data Repository at http://www.stowers.org/research/publications/libpb-1391. The scRNA-seq data generated by Cell Ranger can be retrieved from the GEO database with accession number GSE128306.

References

1. WHO (2004). The global burden of disease: 2004 update.
2. Rook, G.A. (2013). Regulation of the immune system by biodiversity from the natural environment: an ecosystem service essential to health. Proceedings of the National Academy of Sciences of the United States of America *110*, 18360-18367.

3. von Hertzen, L., Hanski, I., and Haahtela, T. (2011). Natural immunity. Biodiversity loss and inflammatory diseases are two global megatrends that might be related. EMBO reports *12*, 1089-1093.
4. Belkaid, Y., and Hand, T.W. (2014). Role of the microbiota in immunity and inflammation. Cell *157*, 121-141.
5. Lambrecht, B.N., and Hammad, H. (2017). The immunology of the allergy epidemic and the hygiene hypothesis. Nature immunology *18*, 1076-1083.
6. Rook, G.A., Martinelli, R., and Brunet, L.R. (2003). Innate immune responses to mycobacteria and the downregulation of atopic responses. Current opinion in allergy and clinical immunology *3*, 337-342.
7. Rosenblum, M.D., Remedios, K.A., and Abbas, A.K. (2015). Mechanisms of human autoimmunity. J Clin Invest *125*, 2228-2233.
8. Lafferty, K.D. (2012). Biodiversity loss decreases parasite diversity: theory and patterns. Philosophical transactions of the Royal Society of London. Series B, Biological sciences *367*, 2814-2827.
9. Kamiya, T., O'Dwyer, K., Nakagawa, S., and Poulin, R. (2014). Host diversity drives parasite diversity: meta-analytical insights into patterns and causal mechanisms. Ecography *37*, 689-697.
10. Herman, A., Brandvain, Y., Weagley, J., Jeffery, W.R., Keene, A.C., Kono, T.J.Y., Bilandzija, H., Borowsky, R., Espinasa, L., O'Quin, K., et al. (2018). The role of gene flow in rapid and repeated evolution of cave-related traits in Mexican tetra, Astyanax mexicanus. Molecular ecology *27*, 4397-4416.
11. Gibert, J., and Deharveng, L. (2002). Subterranean Ecosystems: A Truncated Functional Biodiversity. BioScience *52*.
12. Tabin, J.A., Aspiras, A., Martineau, B., Riddle, M., Kowalko, J., Borowsky, R., Rohner, N., and Tabin, C.J. (2018). Temperature preference of cave and surface populations of Astyanax mexicanus. Developmental biology *441*, 338-344.
13. Abolins, S., King, E.C., Lazarou, L., Weldon, L., Hughes, L., Drescher, P., Raynes, J.G., Hafalla, J.C.R., Viney, M.E., and Riley, E.M. (2017). The comparative immunology of wild and laboratory mice, Mus musculus domesticus. Nature communications *8*, 14811.
14. Trama, A.M., Holzknecht, Z.E., Thomas, A.D., Su, K.Y., Lee, S.M., Foltz, E.E., Perkins, S.E., Lin, S.S., and Parker, W. (2012). Lymphocyte phenotypes in wild-caught rats suggest potential mechanisms underlying increased immune sensitivity in post-industrial environments. Cellular & molecular immunology *9*, 163-174.
15. Prame Kumar, K., Nicholls, A.J., and Wong, C.H.Y. (2018). Partners in crime: neutrophils and monocytes/macrophages in inflammation and disease. Cell Tissue Res *371*, 551-565.
16. Prusall, E.R., and Rolff, J. (2011). Immunopathology and Ecological Immunopathology. In Ecoimmunology, Volume 1st edition. (Oxford University Press), pp. 530-548.
17. Traver, D., Paw, B.H., Poss, K.D., Penberthy, W.T., Lin, S., and Zon, L.I. (2003). Transplantation and in vivo imaging of multilineage engraftment in zebrafish bloodless mutants. Nature immunology *4*, 1238-1246.
18. Pfaffl, M.W., Horgan, G.W., and Dempfle, L. (2002). Relative expression software tool (REST(C)) for group-wise comparison and statistical analysis of relative expression results in real-time PCR. Nucleic Acids Research *30*, 36e-36.
19. Wittamer, V., Bertrand, J.Y., Gutschow, P.W., and Traver, D. (2011). Characterization of the mononuclear phagocyte system in zebrafish. Blood *117*, 7126-7135.
20. R Core Team. (2014). R: A language and environment for statistical computing. (R Foundation for Statistical Computing, Vienna, Austria).
21. Stockdale, W.T., Lemieux, M.E., Killen, A.C., Zhao, J., Hu, Z., Riepsaame, J., Hamilton, N., Kudoh, T., Riley, P.R., van Aerle, R., et al. (2018). Heart Regeneration in the Mexican Cavefish. Cell reports *25*, 1997-2007 e1997.

410 22. Ogryzko, N.V., Renshaw, S.A., and Wilson, H.L. (2014). The IL-1 family in fish: swimming
411 through the muddy waters of inflammasome evolution. Developmental and comparative
412 immunology *46*, 53-62.
413 23. Lugo-Villarino, G., Balla, K.M., Stachura, D.L., Banuelos, K., Werneck, M.B., and Traver,
414 D. (2010). Identification of dendritic antigen-presenting cells in the zebrafish. Proceedings
415 of the National Academy of Sciences of the United States of America *107*, 15850-15855.
416 24. Bolnick, D.I., Shim, K.C., Schmerer, M., and Brock, C.D. (2015). Population-Specific
417 Covariation between Immune Function and Color of Nesting Male Threespine Stickleback.
418 PloS one *10*, e0126000.
419 25. Sunyer, J.O. (2012). Evolutionary and Functional Relationships of B Cells from Fish and
420 Mammals: Insights into their Novel Roles in Phagocytosis and Presentation of Particulate
421 Antigen. Infectious Disorders - Drug Targets *12*, 200-212.
422 26. Peuß, R., Box, A.C., Accorsi, A., Wood, C., Sánchez Alvarado, A., and Rohner, N. (2019).
423 High-throughput, image-based flow cytometry and clustering method for phenotyping
424 heterogeneous cell populations. bioRxiv, 603035.
425 27. van der Meer, W., Scott, C.S., and de Keijzer, M.H. (2004). Automated flagging influences
426 the inconsistency and bias of band cell and atypical lymphocyte morphological
427 differentials. Clin Chem Lab Med *42*, 371-377.
428 28. Rohner, N., Jarosz, D.F., Kowalko, J.E., Yoshizawa, M., Jeffery, W.R., Borowsky, R.L.,
429 Lindquist, S., and Tabin, C.J. (2013). Cryptic variation in morphological evolution: HSP90
430 as a capacitor for loss of eyes in cavefish. Science *342*, 1372-1375.
431 29. Wan, F., Hu, C.B., Ma, J.X., Gao, K., Xiang, L.X., and Shao, J.Z. (2016). Characterization
432 of gammadelta T Cells from Zebrafish Provides Insights into Their Important Role in
433 Adaptive Humoral Immunity. Frontiers in immunology *7*, 675.
434 30. Fan, X., and Rudensky, A.Y. (2016). Hallmarks of Tissue-Resident Lymphocytes. Cell
435 *164*, 1198-1211.
436 31. Mehta, P., Nuotio-Antar, A.M., and Smith, C.W. (2015). gammadelta T cells promote
437 inflammation and insulin resistance during high fat diet-induced obesity in mice. Journal
438 of leukocyte biology *97*, 121-134.
439 32. Xiong, S., Krishnan, J., Peuss, R., and Rohner, N. (2018). Early adipogenesis contributes
440 to excess fat accumulation in cave populations of Astyanax mexicanus. Developmental
441 biology *441*, 297-304.
442 33. Fänge, R., and Nilsson, S. (1985). The fish spleen: structure and function. Experientia *41*,
443 152-158.
444 34. Weisberg, S.P., McCann, D., Desai, M., Rosenbaum, M., Leibel, R.L., and Ferrante, A.W.,
445 Jr. (2003). Obesity is associated with macrophage accumulation in adipose tissue. J Clin
446 Invest *112*, 1796-1808.
447 35. Sheldon, B.C., and Verhulst, S. (1996). Ecological immunology: costly parasite defences
448 and trade-offs in evolutionary ecology. Trends in Ecology & Evolution *11*, 317-321.
449 36. Scharsack, J.P., Kalbe, M., Harrod, C., and Rauch, G. (2007). Habitat-specific adaptation
450 of immune responses of stickleback (Gasterosteus aculeatus) lake and river ecotypes.
451 Proceedings. Biological sciences *274*, 1523-1532.
452 37. Heidt, T., Sager, H.B., Courties, G., Dutta, P., Iwamoto, Y., Zaltsman, A., von Zur Muhlen,
453 C., Bode, C., Fricchione, G.L., Denninger, J., et al. (2014). Chronic variable stress
454 activates hematopoietic stem cells. Nature medicine *20*, 754-758.
455 38. Christ, A., Gunther, P., Lauterbach, M.A.R., Duewell, P., Biswas, D., Pelka, K., Scholz,
456 C.J., Oosting, M., Haendler, K., Bassler, K., et al. (2018). Western Diet Triggers NLRP3-
457 Dependent Innate Immune Reprogramming. Cell *172*, 162-175 e114.
458 39. McAlpine, C.S., Kiss, M.G., Rattik, S., He, S., Vassalli, A., Valet, C., Anzai, A., Chan, C.T.,
459 Mindur, J.E., Kahles, F., et al. (2019). Sleep modulates haematopoiesis and protects
460 against atherosclerosis. Nature.

461

Online Methods section

Fish husbandry

Unless otherwise stated, all fish used for the experiments were adult female fish in the age of 12-16 month. Cave and surface morphs of *Astyanax mexicanus* were reared from Mexican surface fish (Rio Choy) and cavefish originated from the Pachón cave. Fish were housed at a density of ~ 2 fish per liter. The aquatic animal program at the Stowers Institute meets all federal regulations and has been fully AAALAC-accredited since 2005. *Astyanax* are housed in glass fish tanks on racks (Pentair, Apopka, FL) with a 14:10 h light:dark photoperiod . Each rack uses an independent recirculating aquaculture system with mechanical, chemical and biologic filtration and UV disinfection. Water (supplemented with Instant Ocean Sea Salt [Blacksburg, VA]) quality parameters are maintained within safe limits (Upper limit of total ammonia nitrogen range, 1 mg/L; upper limit of nitrite range, 0.5 mg/L; upper limit of nitrate range, 60 mg/L; temperature, 22 °C; pH, 7.65; specific conductance, 800 µS/cm; dissolved oxygen 100 %). Fish were fed once per day with mysis shrimp and twice per day with Gemma diet (according to the manufacturer is Protein 59%; Lipids 14%; Fiber 0.2%; Ash 14%; Phosphorus 1.3%; Calcium 1.5%; Sodium 0.7%; Vitamin A 23000 IU/kg; Vitamin D3 2800 IU/kg; Vitamin C 1000 mg/kg; Vitamin E 400 mg/kg) was fed to adult fish daily at a designated amount of approximately 3% body mass. Routine tank side health examinations of all fish were conducted by dedicated aquatics staff twice daily. *Astyanax* colonies are screened at least biannually for *Edwardsiella ictaluri, Mycobacterium spp., Myxidium streisingeri, Pseudocapillaria tomentosa, Pseudoloma neurophilia*, ectoparasites and endoparasites. At the time of the study, none of the listed pathogens were detected.

In-vitro gene expression analysis

Briefly, single cell suspension from freshly dissected head kidney tissue were produced by forcing tissue through 40 µM cell strainer into L-15 media (Sigma), containing 10 % water and 5 mM

HEPES buffer (pH 7.2) and 20 U/mL heparin (L-90). The strainer was washed once with L-90 and cells were washed once by spinning cells at 500 x *g* at 4 ºC for 5 mins. Supernatant was discarded and cells were resuspended in 1 mL of L-90 media (L-15 containing 10 % water, 5 mM HEPES (7.2 pH), 5 % fetal calf serum, 4 mM L-glutamin, Penicillin-Streptomycin mix with 10000 U/mL each). Cells were counted using EC800 analyser (Sony Biotechnology) and $1x10^6$ cells were plated in 48 'well plate in 500 µL and incubated over night at 21 ºC. At timepoint 0, 20 µg / ml or 0.2 µg / mL lipopolysaccharide mix in PBS (*Escherichia coli* O55:B5 and *E. coli* O111:B4, 1 mg/mL each) or PBS alone as a control was added to the cells, respectively. After 1, 3, 6, 12 and 24 hours, cells were harvested and immediately snap frozen in liquid nitrogen and RNA was isolated as described previously [1]. 100 ng of RNA (concentration was measured using the Qubit system (Thermo Fisher)) from each sample was used for cDNA synthesis using the SuperScript™ III First-Strand Synthesis System kit (Invitrogen) following manufacturer instructions. Resulting cDNA was used for RTqPCR using the PerfeCTa® SYBR® Green FastMix® (Low ROX) (Qunata bio) following manufacturer instructions. Gene specific primers (see Table S1) were used for amplification of target and the two housekeeping genes (rpl32 and rpl13a, see Table S1 for details). Where possible gene specific primer were designed so to span an exon – exon junction. Samples were pipetted in a 384' well plate using a Tecan EVO PCR Workstation (Tecan) and samples were run in technical triplicates on a QuantStudio 7 Flex Real-Time PCR System (Thermo Fisher). Quality control for each sample was performed using the QuantStudio Realt-Time PCR software (Thermo Fisher) and data was exported for analysis in REST 2009 [2] as described before [1]. PBS control samples from each time point and sample was used as the reference to calculate relative expression for target genes for each timepoint and fish, respectively.

Intraperitoneal injection of LPS

Fish were anesthetized using ice cold system water and either PBS (control group) or 20 µg/mL (per g bodyweight) of a LPS mix (*E. coli* O55:B5 and *E. coli* O111:B4, 1 mg/mL each) was injected intraperitoneally using an insulin syringe (3/10 mL, 8 mm length, gauge size 31G, BD). After given timepoints, fish were euthanized using buffered Tricaine solution (500 mg/L) and respective organs were dissected and were either immediately shock frozen for RTqPCR analysis (RNA extraction, cDNA transcription and qPCR was done as described above), fixed in 4 % paraformaldehyde / DEPC water (for tissue RNAscope analysis, see below for details) or forced through a cell strainer (for single cell RNAscope, see below for details) for subsequent analysis.

Phagocytosis Assay

Phagocytosis was performed as previously described [3]. Briefly, single cell solution from freshly dissected head kidney tissue was prepared as described above and $4x10^5$ cells were pipetted into 96' well flat bottom plate and Alexa-488 tagged Staphylococcus aureus (Thermo Fisher) were added in a 1:50 cells / bacteria ratio. To control for cell viability a sample without bacteria was included and to control for active phagocytosis a sample with cells containing bacteria and cytochalasin B (CCB) (0.08 mg /mL) for each individual sample was included. Cells were incubated in 200 µL of L-90 media at 21 ºC for 1 and 3 hours, respectively. To exclude dead cells and signal from non-phagocytosed particles, cells were stained with Hoechst and all samples were quenched using 50 µL Trypan Blue (0.4 % solution, Sigma) before the measurement. Samples were measured on EC800 Analyzer (Sony Biotechnology). Cells were gated for live and Alexa-488 positive and phagocytosis rate was calculated as the ratio of live (Hoechst positive, Excitation 352 nm, Emission 461 nm, FL-6) and phagocytes (Alexa-488 positive, Excitation 495 nm, Emission 519 nm, FL-1) vs. live cells.

Scatter analysis of head kidney

Single cells from head kidney from adult surface fish were extracted as described above. Cells were stained with DAPI to exclude dead cells and live cells were sorted based on populations as described in Fig. 1g using forward side scatter and side scatter characteristics of cells using an Influx System (BD). 1000 cells per population were sorted on a Thermo Scientific™ Shandon™ Polysine Slides and incubated for 30 min at 21 ºC so cells could settle and adhere to slides. Cells were then fixed with 4 % Paraformaldehyde and washed three times in PBS. Cells were then stained using May-Grünwald Giemsa protocol. Briefly, slides were stained for 10 min with a 1:2 solution of May-Grünwald (made in phosphate buffer pH 6.5, filtered), the excess stain was drained off and slides were stained 40 min with a 1:10 solution of Giemsa (made in phosphate buffer pH 6.5, filtered). Then slides were rinsed in ddH20 by passing each slide under running ddH20 10 times. For differentiation, a drop of 0.05 acid water (5ml glacial acetic acid/95ml ddH2O) was put on slide for approx. 4 seconds and quickly rinsed off. Slides were rinsed well, air dried and coverslipped. Only cells that could clearly be identified based on studies in closely related organism using a similar approach [4, 5] were used as representative image for Fig. 1g.

Image-based cluster analysis of head kidney

Briefly, for this analysis, hematopoietic cells from the head kidney were presorted to remove the mature erythrocyte cluster using the S3 Cell Sorter (Bio-Rad) using scatter features (as in Fig. 1e). This was necessary since mature erythrocytes account for about 8 % and 7 % respectively in surface fish and Pachón fish of the entire cell count in the pronephros based on the erythrocyte population we were able to identify using scatter alone (see Fig. 1e). However, based on their biconcave morphology we found erythrocytes in all populations that we could separate through scatter, although mainly in the myelomonocytic and progenitor populations to different degrees

since different orientation in the flow cell of erythrocytes result in different morphological shapes [6]. Based on this, the presence of mature erythrocytes results in massive over-clustering [6]. Reduction of erythrocytes through sorting based on scatter can be used to reduce the amount of over-clustering using the pipeline [6]. Sorted cells were stained with 5 μM Draq5 and 10,000 nucleated, single events were acquired from samples on the ImageStream®X Mark II at 60x, slow flow speed, using 633 nm laser excitation. Bright field was acquired on channels 1 and 9 and Draq5 on channel 11. SSC was acquired on channel 6. Intensities from 25 unique morphological features were extracted. Further analysis was done as described before [6].

Single cell RNAseq

Dissociated hematopoietic cells were stained with DAPI to exclude dead cells and live cells were sorted based on populations as described in Fig. 1g, where only myelomonocyte, lymphocyte and progenitor populations were sorted in L-90 media, to reduce the relative abundance of mature erythrocytes. Sorted cells were spun down (500 x rcf, 4º, 5 min), supernatant was discarded, and cells were resuspended in L-90 media and run again on Influx system to ensure removal of mature erythrocyte cluster and measure cell viability (percentage live cells after sorting: surface fish 82.2 % and cavefish 88.9 %). Cells were loaded on a Chromium Single Cell Controller (10x Genomics, Pleasanton, CA), based on live cell concentration, with a target of 6,000 cells per sample. Libraries were prepared using the Chromium Single Cell 3' Library & Gel Bead Kit v2 (10x Genomics) according to manufacturer's directions. Resulting short fragment libraries were checked for quality and quantity using an Agilent 2100 Bioanalyzer and Invitrogen Qubit Fluorometer. Libraries were sequenced individually to a depth of ~330M reads each on an Illumina HiSeq 2500 instrument using Rapid SBS v2 chemistry with the following paired read lengths: 26 bp Read1, 8 bp I7 Index and 98 bp Read2. Raw sequencing data were processed using 10X Genomics Cell Ranger pipeline (version 2.1.1). Reads were demultiplexed into Fastq file format using cellranger mkfastq.

Genome index was built by cellranger mkref using cavefish genome astMex1, ensembl 87 gene model. Data were aligned by STAR aligner and cell counts tables were generated using cellranger count function with default parameters. Cells with at least 1000 UMI counts were loaded into R package Seurat (version 2.3.4) for clustering and trajectory analysis. 4991 cells for surface and 4103 cells for Pachón cavefish were used for downstream analysis. The UMI count matrix were log normalized to find variable genes. First 12 principal components were selected for dimension reduction and t-SNE plots. Marker genes were used to classify clusters into lymphocytes, myelomonocytes and progenitor types. The results generated by Cell Ranger can be retrieved from the GEO database with accession number GSE128306. The assignment of cell identities is based on their transcription profile determined by similar approaches in zebrafish [4, 7-10]. For the identification of the most common T-lymphocytes population, use of an additional marker was suggested to identify $CD4^+$ helper (T_h-cells) and cytotoxic $CD8^+$ (T_c-cells) T-lymphocytes, since specific monocyte derived populations in other teleost fish species were reported to express *cd4-1* and *cd8a* genes [11]. Here, we used expression of the *sla2* gene that we found to be expressed in all lymphocyte clusters but not in myelomonocyte clusters (see gene enrichment analysis for each cluster in Data File 2).

Il-1β RNAscope assay

Section preparation and RNA in situ hybridization were performed as previously reported [12],[13]. Briefly, for tissue section, respective tissues (head kidney, spleen) were dissected from surface fish and cavefish, followed by immediate immersion into 4% PFA in DEPC H_2O (diluted from 16% (wt/vol) aqueous solution, Electron Microscopy Sciences, cat# 15710) for 24hr at 4°C to fix the tissue, then rinsed well with 1xPBS, dehydrated through graded ethanol (30%, 50%, 70%) and processed with a PATHOS Delta hybrid tissue processor (Milestone Medical Technologies, Inc, MI). Paraffin sections with 8 μm thickness were cut using a Leica RM2255 microtome (Leica

Biosystems Inc. Buffalo Grove, IL) and mounted on Superfrost Plus microscope slides (cat# 12-550-15, Thermo Fisher Scientific). For single cell solutions, head kidney and spleen were dissected, and single cell solutions were produced as described above and approx. 20 µL of the suspension was pipetted on Superfrost Plus microscope slides (cat# 12-550-15, Thermo Fisher Scientific). Cells were allowed to settle for 30 min and fixed using 4% PFA (diluted from 16% (wt/vol) aqueous solution, Electron Microscopy Sciences, cat# 15710) for 1hr at RT, then rinsed well with 1XPBS, dehydrated through graded ethanol (30%, 50%, 70%). RNA in situ hybridization was performed using RNAscope multiplex fluorescent detection V2 kit according to the manufacturer's instructions (Advanced Cell Diagnostics, Newark, CA). RNAscope probe for *il-1β* was a 16ZZ probe named Ame-LOC103026214- C2 targeting 217-953 of XM_022680751.1.

Images of sections were acquired on a Nikon 3PO spinning disc on a Nikon Ti Eclipse base, outfitted with a W1 disk. A 0.75 NA, Plan Apochromat Lambda 20x air objective was used. Dapi and AF647 were excited with a 405 nm and 640 nm laser, respectively, with a 405/488/561/640 nm main dichroic. Emission was collected onto an ORCA-Flash 4.0 V2 digital sCMOS camera, through a 700/75 nm and 455/50 nm filter for the far red channel and DAPI channel, respectively. Z-step spacing was 1.5 microns. All microscope parameters and acquisition were controlled with Nikon Elements software. Identical camera exposure time and laser power was used across samples. All image processing was done with an open source version of FIJI [14] with standard commands. A Gaussian blur with radius of 1 was applied and a rolling ball background subtraction with a radius of 200 pixels was applied to every channel with the exception of the Dapi channel. Following that, a max projection across the slice was applied. For direct comparison, images shown are contrasted identically in the far red (*il-1β*).

Visceral adipose tissue analysis

We dissected the visceral adipose tissue (VAT) from the abdominal cavity as described previously [12]. In short, we manually removed the intestinal sack of the fish and carefully isolated a piece of fat tissue located around the gut for RTqPCR as described above. The rest of the sample was processed as described previously [12]. Briefly, intestine was immediately fixed in 4% paraformaldehyde for 18 h at 4 °C and embedded in JB-4 Embedding solution (Electron Microscopy Sciences; #14270-00) while following kit instructions for dehydration, infiltration and embedding. After sectioning at 5 µm, we dried slides for 1 h in a 60 °C oven and stained slides with hematoxylin for 40 min. After rinsing the slides in PBS, semi-dried slides were stained with eosin (3% made in desalted water) for 3 min. Slides were washed with desalted water and air dried. At least 3 images from VAT of each fish were taken at similar location around the stomach and gut and crown-like structures were scored as described previously [15]. Images were obtained using a 10 x objective on Zeiss Axioplan2 upright microscope and adipocytes and CLS were counted using Adobe Photoshop CC (Version 19.1.0).

Statistical Analysis

Graphical data and statistics were produced using R [16] except otherwise stated. For comparisons between populations we used a one-way ANOVA and corrected for multiple testing against the same control group (FDR) with Holm-Bonferroni test. For analysis of RTqPCR data we used the REST2009 software were significant differences between two groups were determined by a pairwise fixed reallocation randomization test [2]. Phagocytosis data was analyzed using a two-way ANOVA for repeated measurements using Graph Pad Prism Software (Version 8.0.2). To determine significant differences of morphological cell cluster between surface fish and cavefish that resulted from X-shift clustering [17] we used a negative binominal regression model as described before [6].

Animal experiment statement

Research and animal care were approved by the Institutional Animal Care and Use Committee (IACUC) of the Stowers Institute for Medical Research.

References

1. Peuss, R., Eggert, H., Armitage, S.A., and Kurtz, J. (2015). Downregulation of the evolutionary capacitor Hsp90 is mediated by social cues. Proceedings. Biological sciences *282*.
2. Pfaffl, M.W., Horgan, G.W., and Dempfle, L. (2002). Relative expression software tool (REST(C)) for group-wise comparison and statistical analysis of relative expression results in real-time PCR. Nucleic Acids Research *30*, 36e-36.
3. Zhang, Y.A., Salinas, I., Li, J., Parra, D., Bjork, S., Xu, Z., LaPatra, S.E., Bartholomew, J., and Sunyer, J.O. (2010). IgT, a primitive immunoglobulin class specialized in mucosal immunity. Nature immunology *11*, 827-835.
4. Wittamer, V., Bertrand, J.Y., Gutschow, P.W., and Traver, D. (2011). Characterization of the mononuclear phagocyte system in zebrafish. Blood *117*, 7126-7135.
5. Traver, D., Paw, B.H., Poss, K.D., Penberthy, W.T., Lin, S., and Zon, L.I. (2003). Transplantation and in vivo imaging of multilineage engraftment in zebrafish bloodless mutants. Nature immunology *4*, 1238-1246.
6. Peuß, R., Box, A.C., Accorsi, A., Wood, C., Sánchez Alvarado, A., and Rohner, N. (2019). High-throughput, image-based flow cytometry and clustering method for phenotyping heterogeneous cell populations. bioRxiv, 603035.
7. Rowe, R.G., Mandelbaum, J., Zon, L.I., and Daley, G.Q. (2016). Engineering Hematopoietic Stem Cells: Lessons from Development. Cell stem cell *18*, 707-720.
8. Stachura, D.L., Svoboda, O., Campbell, C.A., Espin-Palazon, R., Lau, R.P., Zon, L.I., Bartunek, P., and Traver, D. (2013). The zebrafish granulocyte colony-stimulating factors (Gcsfs): 2 paralogous cytokines and their roles in hematopoietic development and maintenance. Blood *122*, 3918-3928.
9. de Jong, J.L., and Zon, L.I. (2005). Use of the zebrafish system to study primitive and definitive hematopoiesis. Annual review of genetics *39*, 481-501.
10. Athanasiadis, E.I., Botthof, J.G., Andres, H., Ferreira, L., Lio, P., and Cvejic, A. (2017). Single-cell RNA-sequencing uncovers transcriptional states and fate decisions in haematopoiesis. Nature communications *8*, 2045.
11. Nakanishi, T., Shibasaki, Y., and Matsuura, Y. (2015). T Cells in Fish. Biology *4*, 640-663.
12. Xiong, S., Krishnan, J., Peuss, R., and Rohner, N. (2018). Early adipogenesis contributes to excess fat accumulation in cave populations of Astyanax mexicanus. Developmental biology *441*, 297-304.
13. Zeng, A., Li, H., Guo, L., Gao, X., McKinney, S., Wang, Y., Yu, Z., Park, J., Semerad, C., Ross, E., et al. (2018). Prospectively Isolated Tetraspanin(+) Neoblasts Are Adult Pluripotent Stem Cells Underlying Planaria Regeneration. Cell *173*, 1593-1608 e1520.
14. Schindelin, J., Arganda-Carreras, I., Frise, E., Kaynig, V., Longair, M., Pietzsch, T., Preibisch, S., Rueden, C., Saalfeld, S., Schmid, B., et al. (2012). Fiji: an open-source platform for biological-image analysis. Nature methods *9*, 676-682.

15. Sun, K., Park, J., Gupta, O.T., Holland, W.L., Auerbach, P., Zhang, N., Goncalves Marangoni, R., Nicoloro, S.M., Czech, M.P., Varga, J., et al. (2014). Endotrophin triggers adipose tissue fibrosis and metabolic dysfunction. Nature communications *5*, 3485.
16. R Core Team. (2014). R: A language and environment for statistical computing. (R Foundation for Statistical Computing, Vienna, Austria).
17. Samusik, N., Good, Z., Spitzer, M.H., Davis, K.L., and Nolan, G.P. (2016). Automated mapping of phenotype space with single-cell data. Nature methods *13*, 493-496.

Supplemental Figures

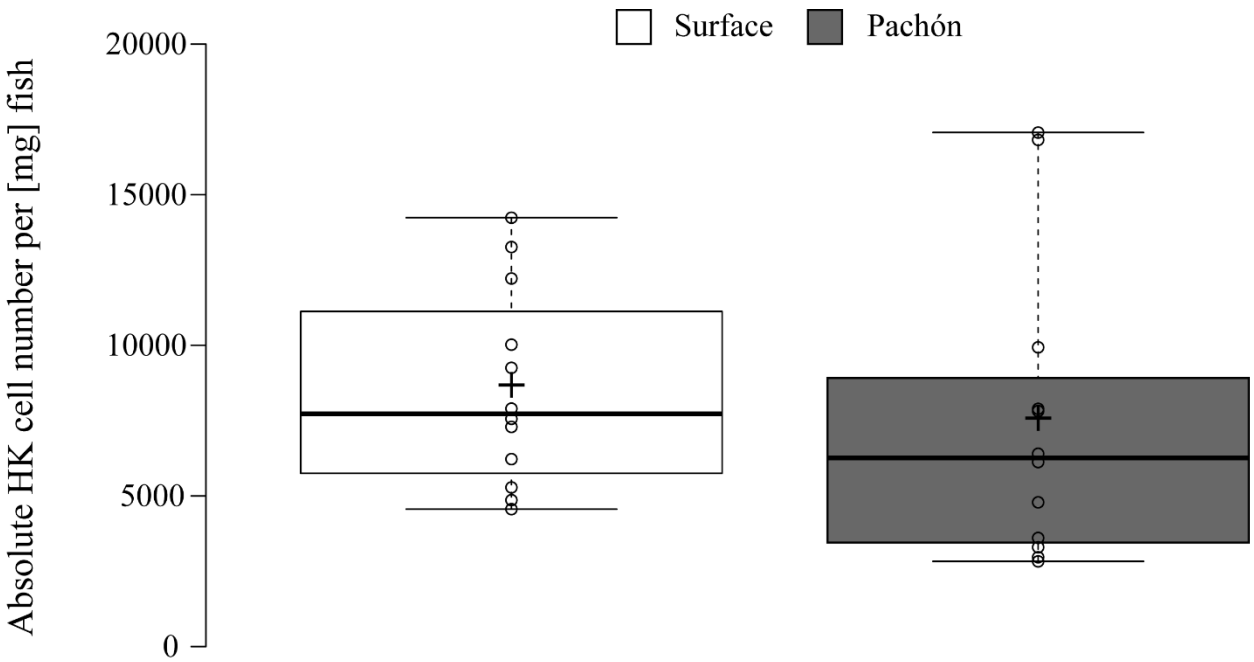

Fig. S1: Total number of head kidney cells from surface fish and cavefish (n=12 for each) relative to fish weight in [mg]. Box plots; center lines show the medians, crosses show means; box limits indicate the 25th and 75th percentiles as determined by R software; whiskers extend 1.5 times the interquartile range from the 25th and 75th percentiles, samples are represented by circles. No statistical difference was detected (p = 0.530409621, One-way ANOVA).

.

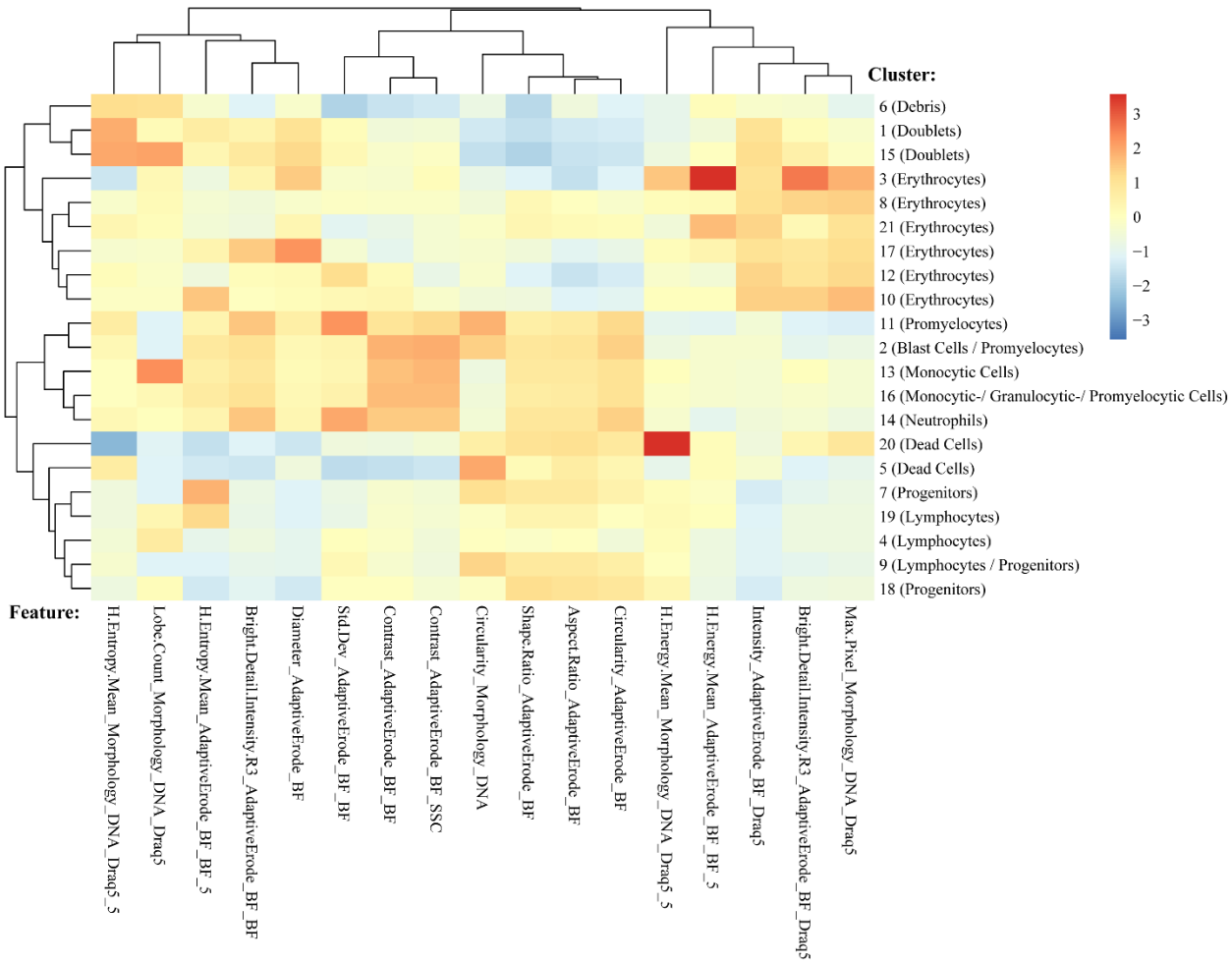

Fig. S2: Spearmen Correlation of overall mean feature intensities used for clustering and single cluster after X-shift based clustering using head kidney cells from surface fish and cavefish. See Table S3 for details of features**.**

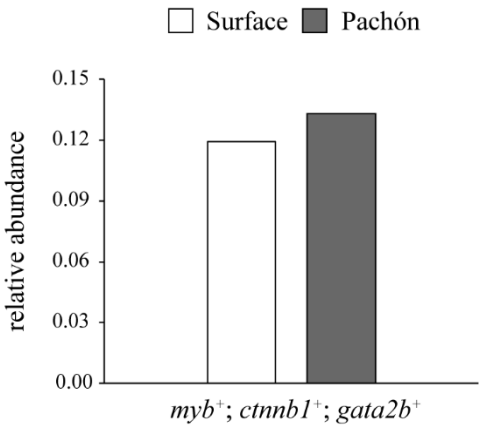

Fig. S3: Relative abundance of hematopoietic stem cells of surface fish and cavefish (Pachón) based on the expression of given gene(s). Cells were assigned to specific population when expressing the respective gene in logFC ≤ 1 in comparison to the overall expression

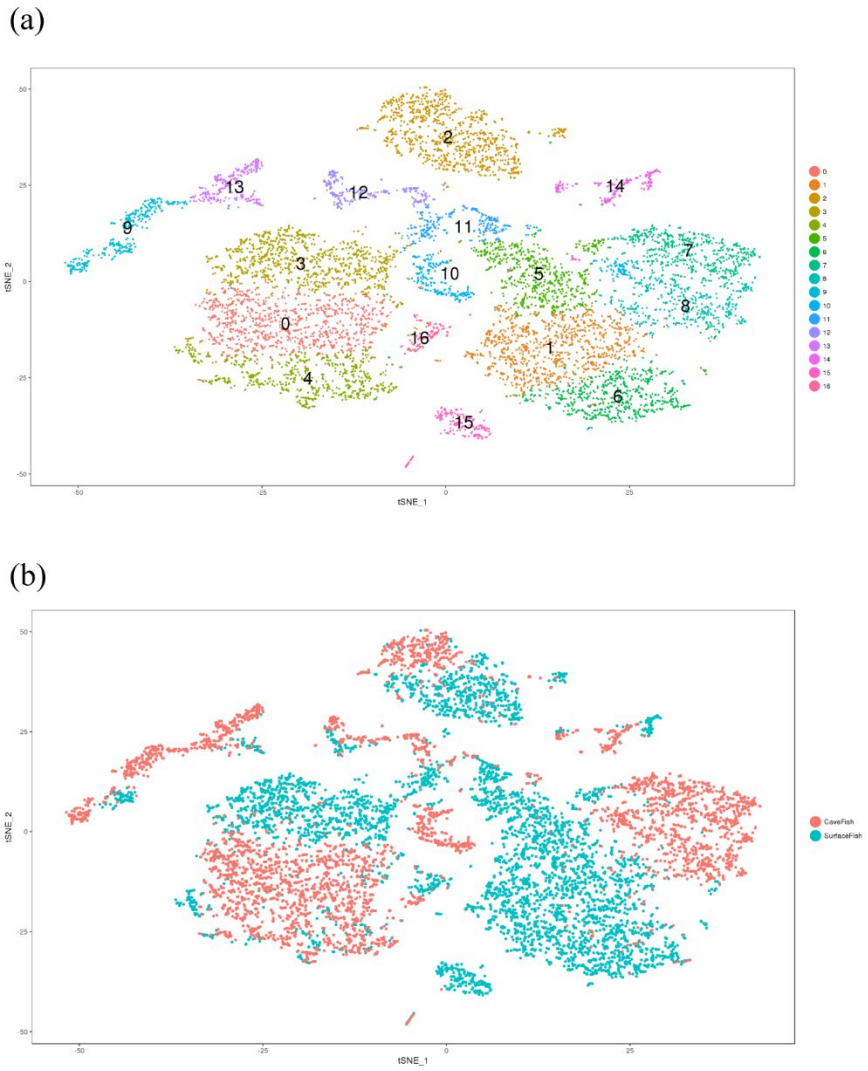

Fig. S 4: t-SNE plots of the first 12 principal components after cluster analysis using R package Seurat (version 2.3.4) for clustering analysis of scRNA-seq data from head kidney from surface fish and cavefish combined. (a) Cluster distribution combining surface fish and cavefish based on gene expression (see Data File 2 for details). (b) Distribution of cavefish and surface fish cells among the 16 cluster.

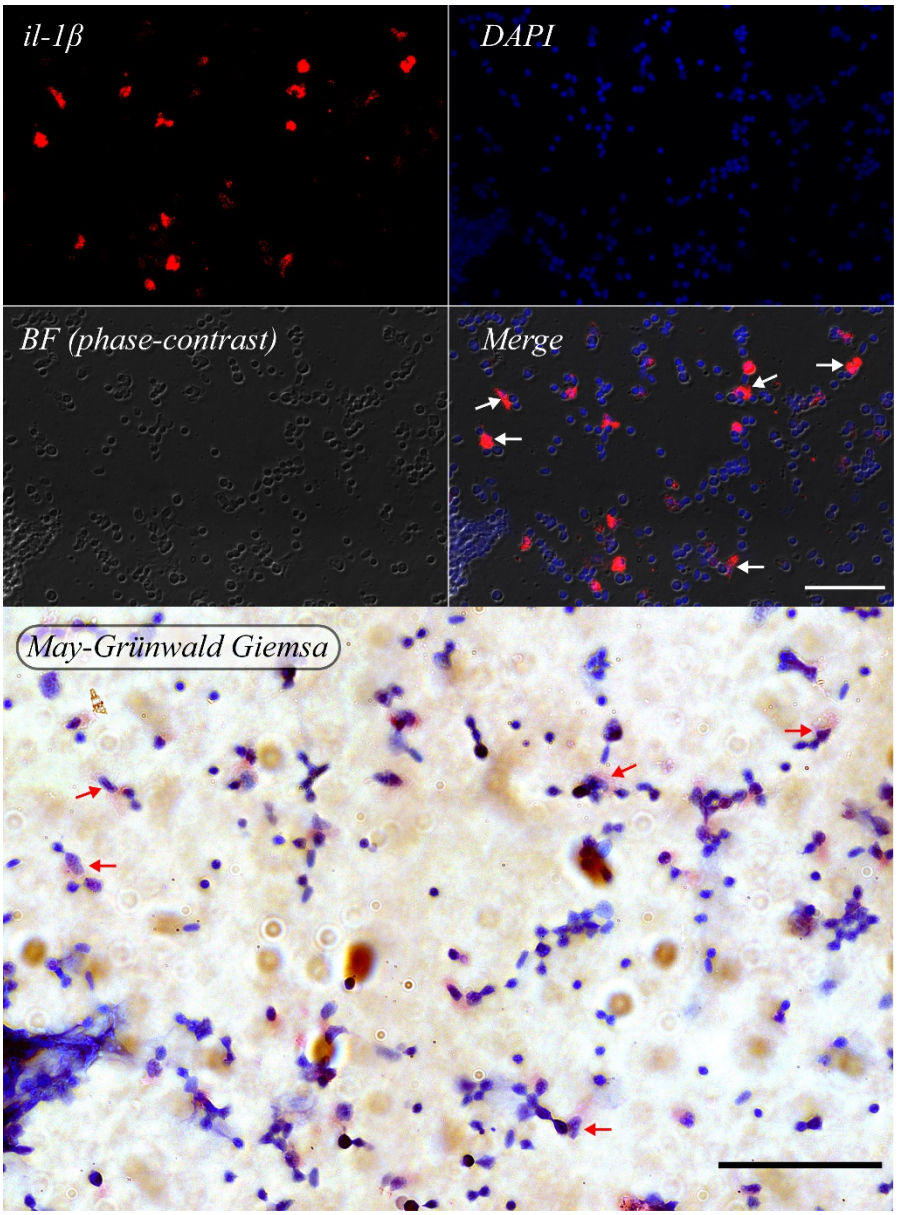

Fig. S 5: RNAscope analysis on dissociated head kidney cells from surface fish 3hpi with LPS (20 µg / g bodyweight). Dissociated cells were transferred on Microscope slide and stained as described in Supplemental Methods. After RNAscope imagining using 700/75 nm and 455/50 nm filter for the far red channel (*il-1β*) and DAPI channel, respectively, cover slip was removed and cells were stained after May-Grünwald Giemsa. Exact position of slide was imaged with 63 X Oil objective as before. Cells expressing *il-1β* are marked with white arrow in '*Merge*' image and the same cells are marked with a red arrow in '*May-Grünwald Giemsa*' image.

Supplemental Tables

Table S1: Primer-sequences with respective efficiencies (E) for RT-qPCR.

Gene Symbol	Name	Gene Accession Number	E / Fragment length bp	5' – 3' primer sequence	Primer origin
Il-1β	*Interleukin 1 beta*	XM_022680751	1.99 / 78	F: AGGAAACCAGAGTCAGAGCG R: GGCTGACCCTTTGTGGAGTT	This study
tnf-α	*Tumor necrosis factor alpha*	XM_015602024	1.97 / 154	F: TCTGGCTATAGCTGTGTGCG R: TGGGTTGTAGTGACCTGACA	This study
Il-6	*Interleukin 6*	XM_022668071	1.99 / 116	F: CTGCGGGATGAGCAGTTTCA R: TTGTGTCGGCACCTGTCTTC	This study
g-csf	*Granulocyte colony froming factor*	XM_007255159	1.95 / 138	F: TGCAGAATCCTGCCTTCGAG R: GTTTGCCTGAGTCATTGCCG	This study
rpl32	*Ribosomal protein L32*	XM_007251493	1.99 / 144	F: CGCTTTAAGGGACAGATGCT R: GTAGCTCTTGTTGCTCATCA	This study
rpl13a	*Ribosomal protein L13a*	XM_007244599	1.99 / 147	F: TCTGGAGGACTGTAAGAGGTATGC R: AGACGCACAATCTTGAGAGCAG	Beale, Guibal [1]

1. Beale, A. *et al.* Circadian rhythms in Mexican blind cavefish Astyanax mexicanus in the lab and in the field. *Nature communications* **4**, 2769 (2013).

Table S2: Results from two-way ANOVA for repeated measurements comparing phagocytosis rates over time (1 h & 3 h) between surface and cavefish

Term	SS	DF	MS	F (DFn, DFd)	P value
Interaction (Time x Fish)	0.003328	1	0.003328	F (1, 10) = 3.771	P=0.0808
Time	0.01241	1	0.01241	F (1, 10) = 14.07	P=0.0038
Fish	0.07053	1	0.07053	F (1, 10) = 59.98	P<0.0001
Subject	0.01176	10	0.001176	F (10, 10) = 1.332	P=0.3293
Residual	0.008824	10	0.000882		

Table S3: Overview of features extracted for morphological identification of *A. mexicanus* head kidney cells.

Feature ID	Feature_ImageMask_Channel	Feature description
1	Area_AdaptiveErode_BF	Cell size
2	Area_Intensity_SSC	Areas of SSC signal above background
3	Area_Morphology_DNA	Area of DNA signal (nuclear staining)
4	Aspect.Ratio_AdaptiveErode_BF	Aspect ratio of total cell area
5	Bright.Detail.Intensity.R3_AdaptiveErode_BF_BF	Intensity of brightest staining areas
6	Bright.Detail.Intensity.R3_AdaptiveErode_BF_Draq5	Intensity of brightest staining areas
7	Bright.Detail.Intensity.R3_AdaptiveErode_BF_SSC	Intensity of brightest signal areas
8	Circularity_AdaptiveErode_BF	Circularity of whole cell shape
9	Circularity_Morphology_DNA	Circularity of nucleus
10	Contrast_AdaptiveErode_BF_BF	Detects large changes in pixel values - can be measure of granularity of signal
11	Contrast_AdaptiveErode_BF_SSC	Detects large changes in pixel values - can be measure of granularity of signal
12	Diameter_AdaptiveErode_BF	Diameter of whole cell shape
13	Diameter_Morphology_DNA	Diameter of nucleus
14	H.Energy.Mean_AdaptiveErode_BF_BF_5	Measure of intensity concentration - texture feature
15	H.Energy.Mean_Morphology_DNA_Draq5_5	Measure of intensity concentration - texture feature
16	H.Entropy.Mean_AdaptiveErode_BF_BF_5	Measure of intensity concentration and randomness of signal - texture feature
17	H.Entropy.Mean_Morphology_DNA_Draq5_5	Measure of intensity concentration and randomness of signal - texture feature
18	Intensity_AdaptiveErode_BF_Draq5	Integrated intensity of signal within whole cell mask
19	Intensity_AdaptiveErode_BF_SSC	Integrated intensity of signal within whole cell mask
20	Lobe.Count_Morphology_DNA_Draq5	Number of lobes of nucleus
21	Max.Pixel_Intensity_Ch6_SSC	maximum pixel intensity of stated channel within a whole cell mask
22	Max.Pixel_Morphology_DNA_Draq5	maximum pixel intensity of stated channel within a whole cell mask
23	Mean.Pixel_Morphology_DNA_Draq5	mean pixel intensity of stated channel within a whole cell mask
24	Shape.Ratio_AdaptiveErode_BF	minimum thickness divided by length - measure of cell shape characterisic
25	Std.Dev_AdaptiveErode_BF_BF	standard deviation of BF signal - measure of granularity and variance in BF